Supplementary Data for

Metastasis and immune evasion from extracellular cGAMP hydrolysis

SUPPLEMENTARY METHODS

The generation of knockout cell lines: Murine cancer cells deficient in *Cgas*, or *Enpp1* were generated by Cas9 ribonucleoprotein nucleofection using a Lonza 4D-Nucleofector and SF Cell line Kit. crRNA (IDT) sequences is listed in Supplementary Table S1. Four guides were screened per target and knockout cell lines were confirmed using immunoblotting. Antibody information used in immunoblotting experiments is listed in Supplementary Table S2. Stable knockdown of ENPP1 in MDA-MB-231 cells was achieved using shRNAs in pRRL (SGEP or SGEN) plasmids obtained from the MSKCC RNA Interference Core. Four distinct shRNA hairpins were screened per target. Targeted shRNA sequences are listed in Supplementary Table S1.

Immunofluorescence microscopy: Cells were fixed with ice-cold (−20 °C) methanol for 15 min (when staining for centromeres and cGAS) or 4% paraformaldehyde (when staining for GFP). Subsequently, cells were permeabilized using 1% triton for 4 min. See Supplementary Table S3 for antibody information. TBS–BSA was used as a blocking agent during antibody staining. DAPI was added together with secondary antibodies. Cells were mounted with Prolong Diamond Antifade Mountant (Life Technologies, P36961).

Immunoblotting: Cells were pelleted and lysed using RIPA buffer. Protein concentration was determined using BCA protein assay and 20–30 μg total protein were loaded in each lane. Proteins were separated by gradient SDS–PAGE and transferred to PVDF or nitrocellulose membranes. See Supplementary Table S2 for antibody information. Membranes were imaged using the LI-COR Odyssey software.

ENPP1 staining of human xenografts: Immunohistochemistry for ENPP1 in human breast cancer xenografts was performed on the automated Discovery XT processor (Ventana Medical Systems) by the Molecular Cytology Core Facility at MSKCC. Briefly, after deparaffinized and tumor tissue conditioning, the antigen was retrieved using sodium citrate pH6 buffer for 30 min. Following blockage with Background Buster (Innovex), the slides were incubated with 2.5 μg/ml anti-ENPP1 antibody (Abcam ab4003 at 1:200, Supplementary Table S4) for 4 hr, and then incubated with the biotinylated secondary antibody for 30 minutes. The Streptavidin-HRP D (DABMap kit, Ventana Medical Systems) and the DAB detection kit (Ventana Medical Systems) were used to detect the signal according to the manufacturer instructions. Then the slides were counterstained with hematoxylin and were mounted with Permount mounting medium. Tumor necrosis was assessed semi quantitatively by a certified pathologist based on the cross-sectional area containing necrosis. The pathologist was blinded to tumor group allocation.

Quantitative PCR: RNA was extracted from cells with Trizol (Invitrogen #15596026). cDNA was synthesized using the RNA to cDNA EcoDry™ Premix (Double Primed) kit (Takara #639549). Real-time PCR was performed to measure the relative mRNA expression levels of *Enpp1* and the control *Gapdh* using Luna® Universal qPCR Master Mix (NEB M3003L). The qPCR reaction

and analysis were performed on a QuantStudio 6 platform (Life technology). Two sets of primers for *Enpp1* were used. The sequence for one set of primers is 5'-CTGGTTTTGTCAGTATGTGTGCT-3' and 5'-CTCACCGCACCTGAATTTGTT-3' and the sequence for another set of primers is 5'-CTTTGAAAGGACGTTCAGCAAC-3' and 5'-AGGAGCACACGAACCTGGA=3'. The sequence for primers for GAPDH is 5'-AGGTCGGTGTGAACGGATTTG-3' and 5'-TGTAGACCATGTAGTTGAGGTCA-3'.

Cellular growth and migration assays: Cellular proliferation rates were assessed by seeding 2.5 x 10^4 control or *Enpp1*-KO 4T1 cells in 6-well plates (3-4 replicates per condition). For migration assays, cells were seeded in the regular RPMI medium with 10% Fetal bovine serum (FBS). About 48 hours before cells growing to form a 90% confluency monolayer, regular media were replaced with media containing indicated drugs. The working concentration of cGAMP, adenosine, and the A2B antagonist PSB115 was 5.5 μM, 5.5 μM, and 1 μM, respectively. Fresh medium was changed every 12 hours. When reaching ~ 90% confluency, cells were treated with RPMI medium containing 10 μM Mitomycin C for 1 hour. Wounds were formed using sterile P200 pipette tips for experiments using 4T1 and CT26 cells and directly using wound-healing inserts (IBIDI) for experiments using E0771 cells. Adenosine deaminase was used at concentration of (1 IU/ml) and added daily. Images of the wounds were captured every 8 hours and were analyzed with a wound healing tool macro in ImageJ (http://dev.mri.cnrs.fr/projects/imagej-macros/wiki/Wound_Healing_Tool).

Analysis of ENPP1 protein expression and tumor infiltrating lymphocytes in breast tumor samples: Primary analysis of ENPP1 protein expression was performed on a tissue microarray (TMA) of comprising 226 TNBC FFPE tumor samples of which 223 had sufficient material. Samples and follow up data for cohort 1 were collected MSKCC IRB approval. There were 3 cores per tumor sample. Detailed clinical characteristics and clinical follow-up data were previously reported (1). Immunohistochemistry for ENPP1 in breast cancer cohort 1 was performed on the automated Discovery XT processor (Ventana Medical Systems) by the Molecular Cytology Core Facility at MSKCC. Briefly, after deparaffinized and tumor tissue conditioning, the antigen was retrieved using standard CC1 (Ventana Medical Systems). Following blockage with Background Buster (Innovex), the slides were incubated with 2.5 μg/ml anti-ENPP1 antibody (ab245838, Abcam) for 5 hr, and then incubated with the biotinylated secondary antibody for 60 minutes. The Streptavidin-HRP D (DABMap kit, Ventana Medical Systems) and the DAB detection kit (Ventana Medical Systems) were used to detect the signal according to the manufacturer instructions. Then the slides were counterstained with hematoxylin and were mounted with Permount mounting medium. Slides of immunofluorescence and immunohistochemistry were scanned with Pannoramic Flash 250 (3DHistech, Budapest, Hungary) with 20x/0.8 NA air objective by the Molecular Cytology Core Facility at MSKCC. ENPP1 protein expression levels were performed by a board-certified breast pathologist who was blinded to other clinicopathological characteristics and outcome. ENPP1 protein expression levels were assessed manually using scores of 0 (absent), 1 (weak), 2 (moderate) and 3 (strong) for both stromal and tumor compartments. Given this analysis was performed on small core material, ENPP1 expression was considered when >1% of cells showed a given staining pattern. Distant metastasis-free survival data were collected by reviewing medical records available at MSKCC. TILs were scored according to the recommendations of the international TILs working group (2) based on the original hematoxylin and eosin-stained sections corresponding to each of the tumors present in the TMA. Tumors were stratified as having low (negative or weak) or high (moderate or strong) ENPP1 expression. Independent validation studies were performed on a tissue microarray of n = 91 estrogen receptor (ER) negative (Cohort 2)

and n= 115 ER positive (Cohort 3) FFPE breast tumors identified by the Northern Ireland Biobank (NIB), previously described elsewhere (3,4). Resected tumors were available between 1998 and 2008, with long-term follow-up data (relapse-free and overall survival) collated via the Northern Ireland Cancer Registry. Immunohistochemistry (IHC) was performed on 4 μm sections for CD8 (NIB15-0168, Office for Research Ethics Committees Northern Ireland (ORECNI) 13-NI-0149) using C8/144B, M7103, Dako at 1:50 dilution after an ER2 20 minutes retrieval, and for ENPP1 (NIB19-0301, ORECNI 13-NI-0149) using anti-ENPP1 antibody (ab245838, Abcam) at 1:1000 dilution. Slides were scanned on an Aperio AT2 Digital scanner at 40x. CD8+ T cell infiltration was reported as CD8+ cell density per mm^2 based on the total number of cells in each core and determined using the open-source digital pathological analysis software QuPath *v0.1.2* (5,6). Cores with < 100 tumor cells were removed from analysis and multiple core data were averaged. Rigorous quality control steps were taken to remove necrosis or keratin, tissue folds and entrapped normal structures; this was confirmed by a second reviewer with frequent consultation following an established method. ENPP1 protein expression levels were assessed manually using scores of 0 (absent), 1 (weak), 2 (moderate) and 3 (strong) for both stromal and tumor compartments as described above. Both analyses were performed blinded to other clinicopathological characteristics and outcome. Survival analysis was restricted to tumors with low nodal disease burden (N0-1). For OS analysis, ER- tumors were stratified as either positive (n= 59) or negative (n = 15) for ENPP1 staining. Given increased expression of ENPP1 in ER+ tumors in general, tumors were stratified as either having low (negative, weak, or moderate, n = 41) or high (strong, n = 42) ENPP1 staining.

ENPP1 staining and immune profiling of mucosal melanoma samples: Immunofluorescence for ENPP1 and cGAS was performed on the automated Discovery XT processor (Ventana Medical Systems) by the Molecular Cytology Core Facility at MSKCC (7). The procedure of deparaffinization, cell condition, antigen retrieval, and nonspecific blockages was similar as described in the immunohistochemistry section above. Instead of DAB detection kit, Tyramide-Alexa Fluor 488 (Invitrogen B40932) and Tyramide-Alexa Fluor 594 (Invitrogen B40957) were used for signal detection. cGAS and ENPP1 staining were sequentially performed with 1:200 diluted anti-cGAS and 1 ug/ml of anti-ENPP1 antibodies as the primary antibodies. DNA was stained with 5 μg/ml of DAPI in PBS for 10 minutes. Then the slides were mounted with Mowiol mounting medium.

RNAseq analysis of human sarcomas: Matched clinicopathological and RNA sequencing data for samples annotated as undifferentiated pleomorphic sarcoma (UPS, also known as malignant fibrous histiocytoma) were obtained from The Cancer Genome Atlas (TCGA) Genomic Data Commons Data Portal repository in May 2018. Raw read counts were utilized for our analysis. Two additional publicly available RNA sequencing datasets of UPS tumors were obtained for validation (8,9). For analysis of the Steele et *al*. dataset (EGAD00001004439), we utilized previously processed data (transcripts per million). For analysis of the Lesluyes et *al*. dataset, FASTQ files (SRA accession ID SRP057793) were preprocessed with Kallisto (10) using the human genome reference GRCh38 and transcript level abundances were computed using the Bioconductor package tximport (11). The abundance of tissue-infiltrating immune cells was estimated using transcriptome-based methods. The Microenvironment Cell Populations-counter (MCP-counter) method (12) was used to determine relative abundance of various tumor immune microenvironment constituents. Specifically, MCP-counter cytotoxic T-lymphocyte (CTL) scores were calculated from expression of seven transcripts including *CD8A* and log2-normalized. CTL scores were validated using an

orthogonal transcriptome-based method, cytolytic activity (CYT) scores (13), calculated as the geometric mean of granzyme A (*GZMA*) and perforin (*PRF1*) transcript counts.

Bladder cancer response data to anti-PD-L1 treatment: RNA sequencing data was obtained from Mariathasan et *al*. (32), a metastatic urothelial cancer anti-PD-L1 treated cohort in SRA format, and reverted back to FASTQ using bam2fastq (v1.1.0). FASTQ reads were aligned to the hg19 genome using STAR (14). Transcript quantification was performed using RSEM with default parameters (15). Response was defined based on radiological response as per the RECIST criteria, with "CR/PR" being classified as a responder and "SD/PD" being a non-responder. The $CGAS^{high}$ group was defined as the upper two tertiles, and $CGAS^{low}$ as the bottom tertile, of *CGAS* expression.

SUPPLEMENTARY FIGURES AND FIGURE LEGENDS

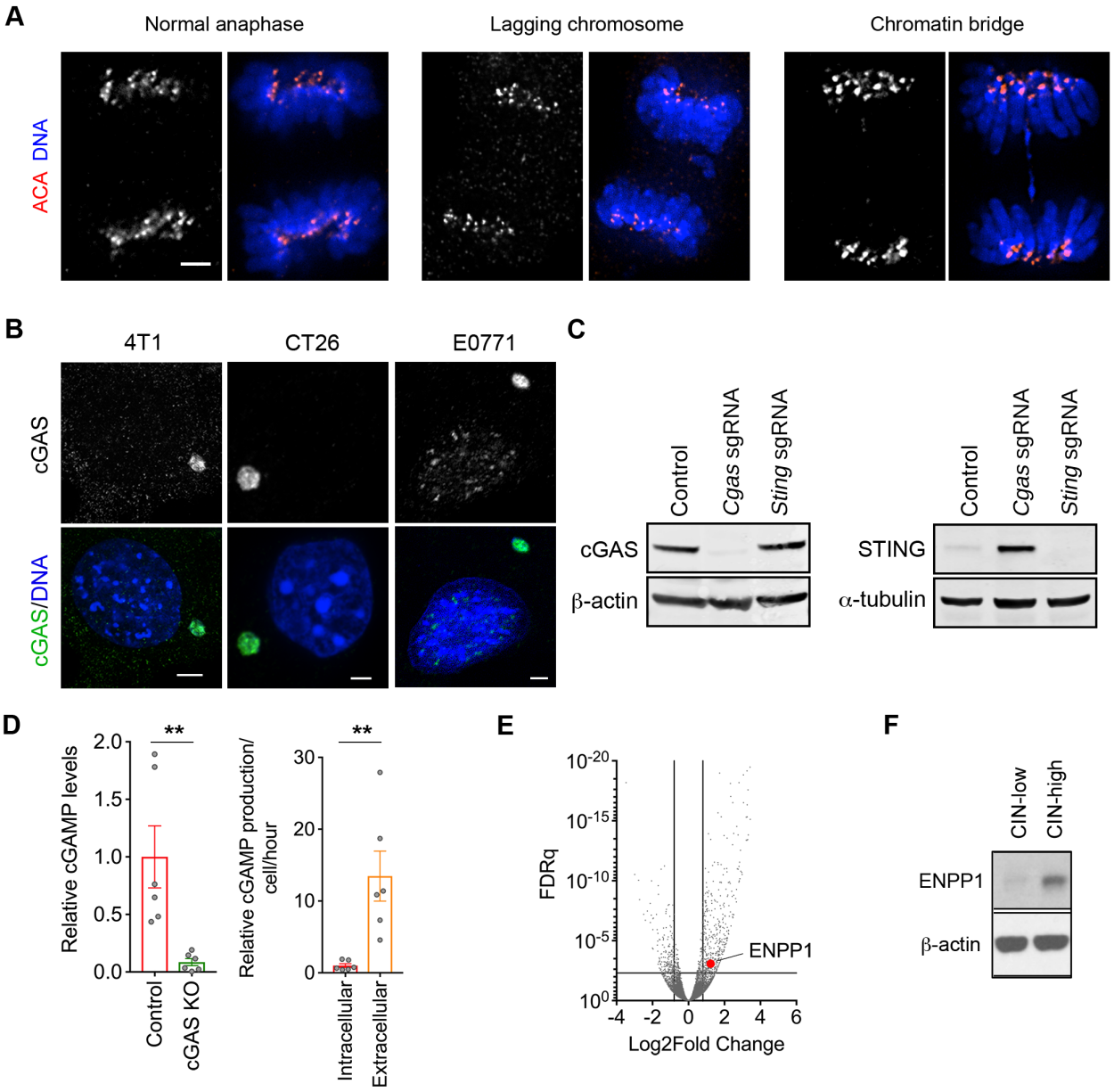

Supplementary Figure S1. (A) Representative images of 4T1 cells undergoing error-free anaphase or anaphase with evidence of chromosome missegregation, scale bar 2μm. (B) Representative image of a 4T1, CT26, and E0771 cells with micronuclei stained using DAPI and anti-cGAS antibody, scale bar 2μm. (C) Immunoblots of control, *Cgas*-KO, and STING(*Tmem173*)-KO 4T1 cell lysates stained using anti-STING, anti-cGAS, α-tubulin and β-actin antibodies. (D) *Left,* cGAMP levels in cell lysates of 4T1 cells incubated in serum-free media for 24 hours. cGAMP levels were normalized for cell number. *Right*, Relative intracellular and extracellular cGAMP production in 4T1 cells. Bars represent mean ± s.e.m. n = 6 independent experiments ** p<0.01, two-sided t-test. (E) Volcano plot showing differentially expressed genes between MDA-MB-231 cells expressing MCAK or Kif2b (CIN^{low}) or dominant-negative MCAK (CIN^{high}). (F) Immunoblots of CIN^{low} and CIN^{high} cell lysates stained with anti-ENPP1 and anti-β-actin antibodies.

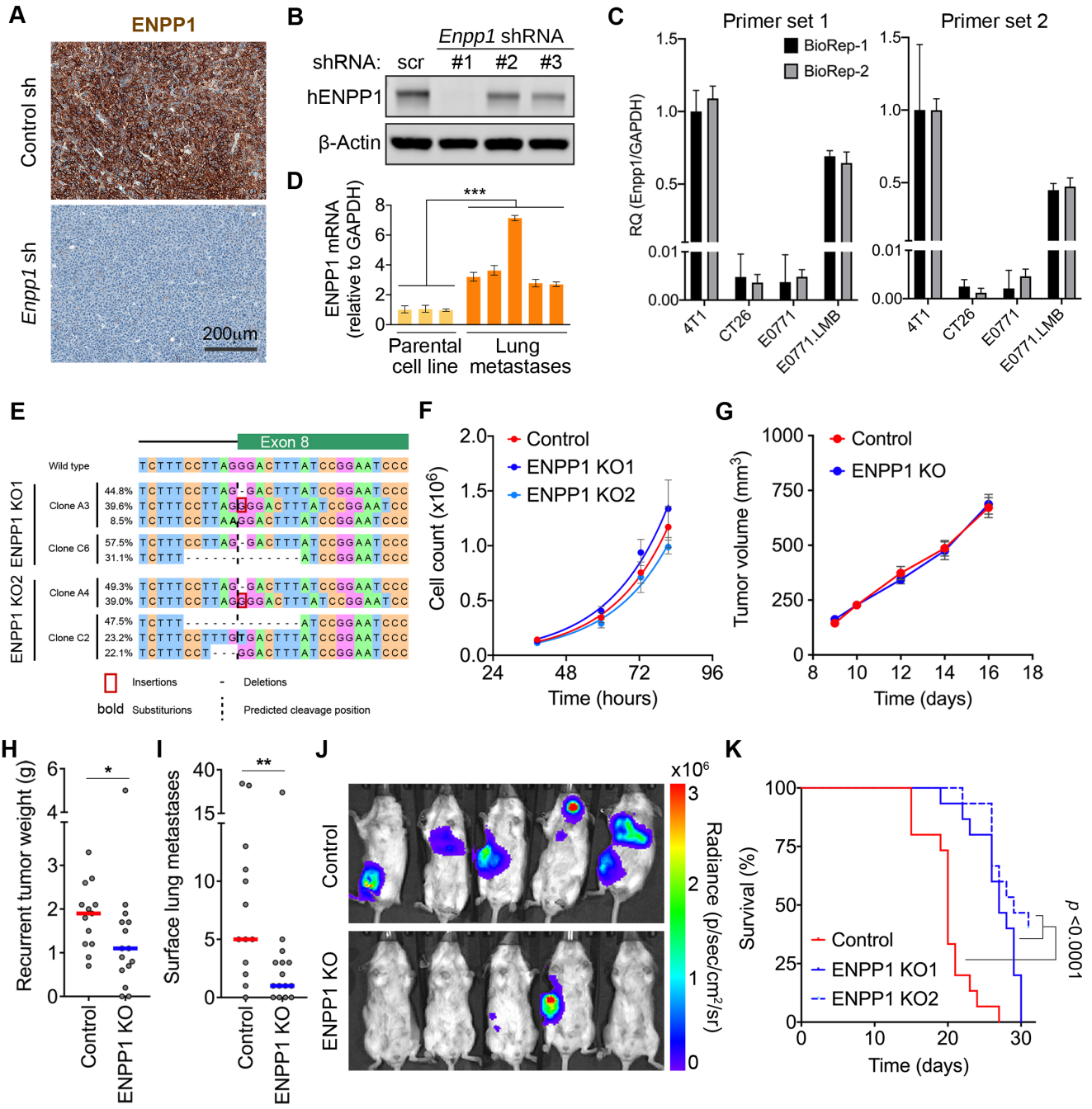

Supplementary Figure S2. (A) Representative immunohistochemistry (IHC) images of control and ENPP1-depleted orthotopically transplanted human TNBCs stained using anti-ENPP1 antibody, scale bar 200μm. (B) Immunoblots of control and ENPP1-depleted CIN^{high} MDA-MB-231 cell lysates stained using anti-ENPP1 and anti-β-Actin antibody. (C) Relative ENPP1 mRNA levels in 4T1, CT26, E0771, E0771.LMB cells. (D) ENPP1 mRNA levels in 4T1 cells as well as cells derived from lung metastases. ***$p < 0.001$, two-tailed t-test. (E) Sequence of 4T1 single-cell derived clones showing successful ENPP1 knockout and absence of wildtype allele. (F) Proliferation of control and *Enpp1*-knockout 4T1 cells over time. (G) Volume of orthotopically transplanted control and ENPP1-knockout tumors over time. Data points represent average ± s.e.m. (H-I) Recurrent primary tumor weight (H) and surface lung metastases (I) after resection of control or *Enpp1*-knockout primary tumor resection, bars represent median, * $p<0.05$, ** $p<0.01$, two-sided Mann-Whitney test. (J) Representative bioluminescence

images of BALB/c mice 35 days after orthotopic transplantation with control and *Enpp1*-KO 4T1 tumors followed by tumor resection on day 7. (K) Overall survival of animals injected by control or *Enpp1* knockout 4T1 cells, n = 15 animals per condition, significance tested using log-rank test.

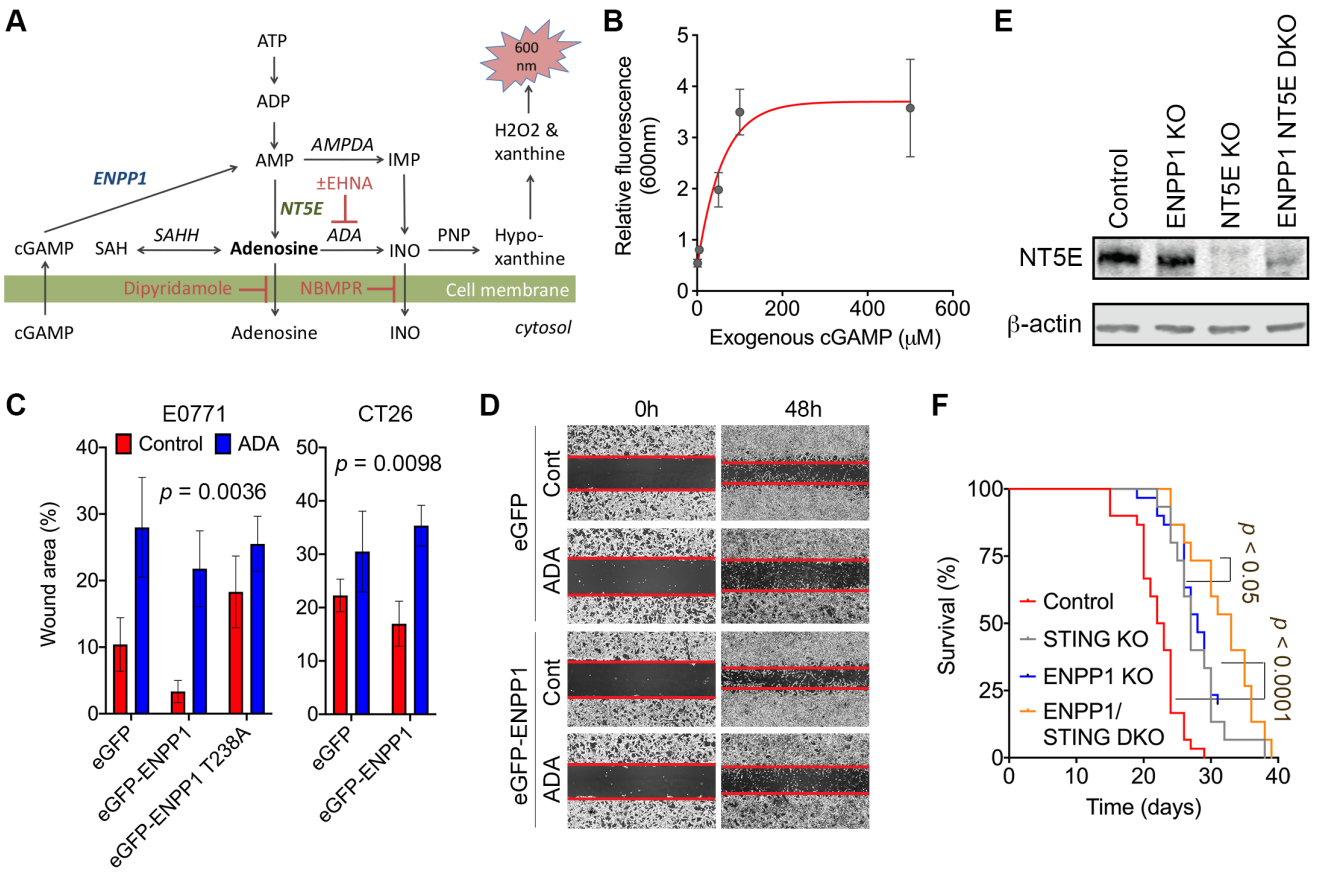

Supplementary Figure S3. (A) Schematic of extracellular adenosine metabolism illustrating an indirect fluorescence-based method of quantifying extracellular adenosine production. By subtracting fluorescence measurements obtained from media containing adenosine deaminase inhibitor, PSB115, from media without the inhibitor, we are able to quantify the amounts of downstream products arising from extracellular adenosine degradation. (B) Relative fluorescence intensity at 600 nm with and without the addition of PSB115 in the presence of increasing amounts of exogenous cGAMP. (C) Immunoblots of control, *Enpp1*-KO, *Nt5E*-KO, and *Enpp1*/*Nt5e* double-KO 4T1 cell lysates stained using anti-NT5E and β-Actin antibodies. (D) Percent wound remaining after 48 hours in CT26 and E0771 cells expressing eGFP, eGFP-ENPP1, or eGFP-ENPP1-T328A treated with or without Adenosine deaminase inhibitor (ADA), bars represent mean ± s.e.m., n = 5-6 biological replicates (E0771) and 15 replicate (CT26), significance tested using ANOVA. (E) Representative images of wounds at 0 hr and 48 hr with or without ENPP1 expression and ADA treatment. (F) Overall survival of animals injected by control, *Enpp1*-KO, STING-KO, or Enpp1/*STING* double-KO 4T1 cells, n = 15 animals per condition, significance tested using log-rank test.

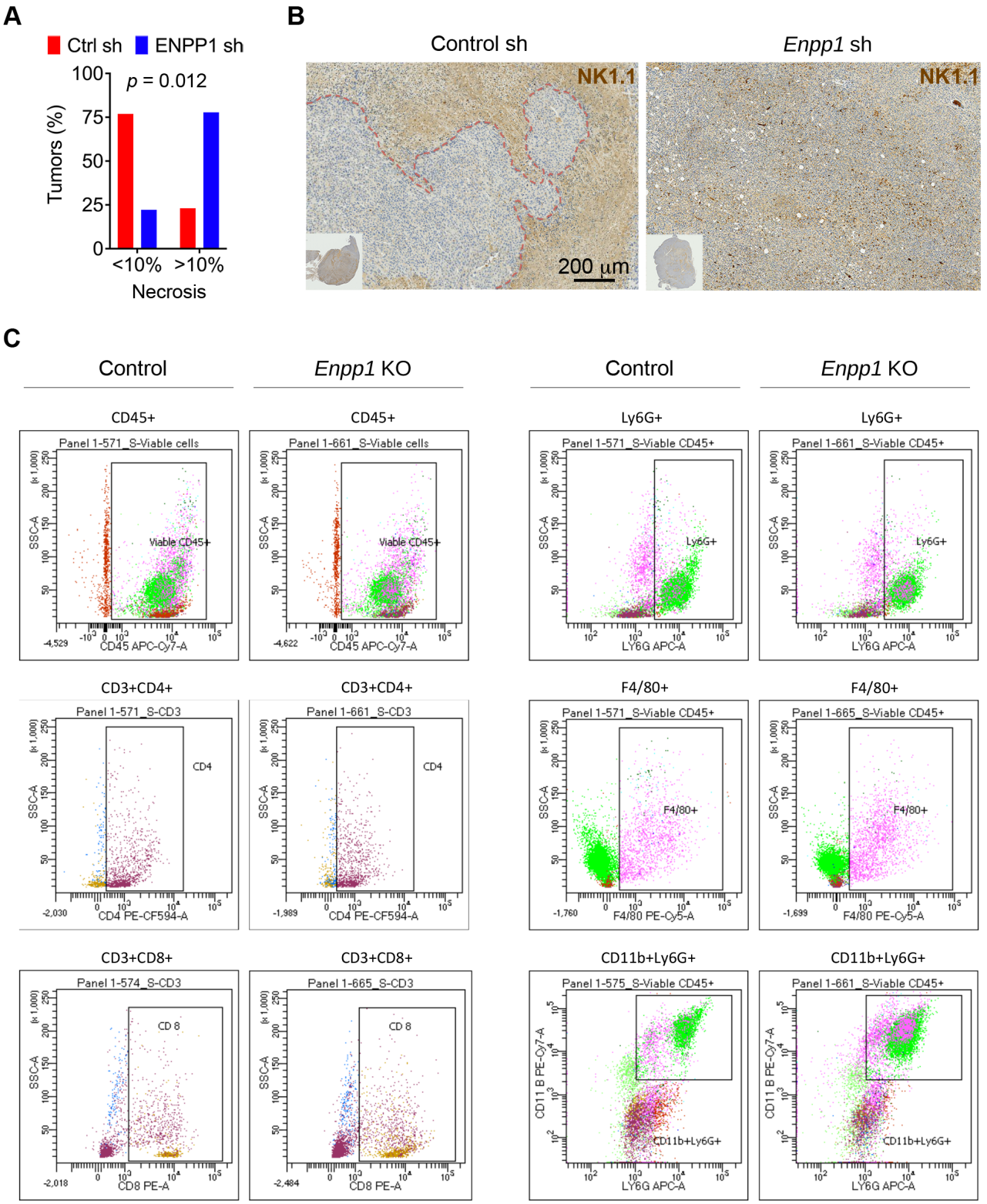

Supplementary Figure S4. (A) Semi-quantitative measurement of tumor necrosis in control and ENPP1-depleted human TNBC xenografts. (B) Representative IHC images of control and ENPP1-depleted TNBC xenografts stained using NK1.1 (to stain NK-cells), scale bar 200μm. (C) FACS gating scheme for immune profiling experiments of dissociated lungs containing control and *Enpp1*-KO lung metastasis from 4T1 tumors.

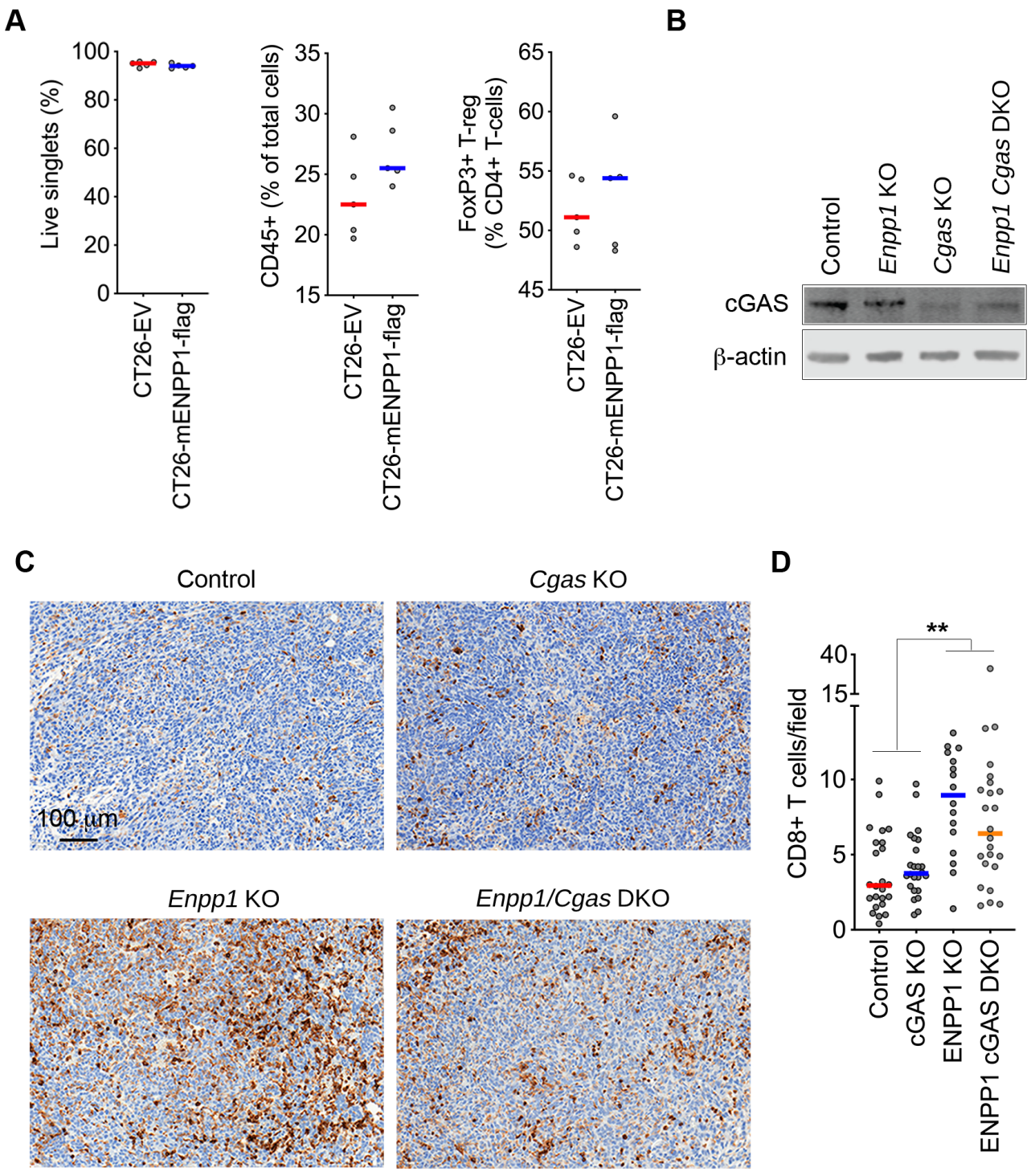

Supplementary Figure S5. (A) Percentage of live cells, CD45+ cells, and FoxP3+ CD4+ T-cells obtained from dissociated sub-cutaneously transplanted control and ENPP1 expressing CT26 tumors, n = 5 animals per group, bars represent median, * $p < 0.05$. (B) Immunoblots of control, *Enpp1*-KO, *Cgas*-KO, and *Enpp1*/*Cgas* double-KO 4T1 cell lysates stained using anti-cGAS and β-Actin antibodies. (C) Representative immunohistochemistry (IHC) of control, *Enpp1*-KO, *Cgas*-KO, and *Enpp1*/*Cgas* double-KO 4T1 lung metastases stained using an anti-CD45 antibody. (F) The number of CD8+ T-cells per field (4000μm^2) in

control, *Enpp1*-KO, *Cgas*-KO, and *Enpp1*/*Cgas* double-KO 4T1 lung metastases, bars represent median, n = 17-26 fields, **** $p<0.01$, two-sided Mann-Whitney test.

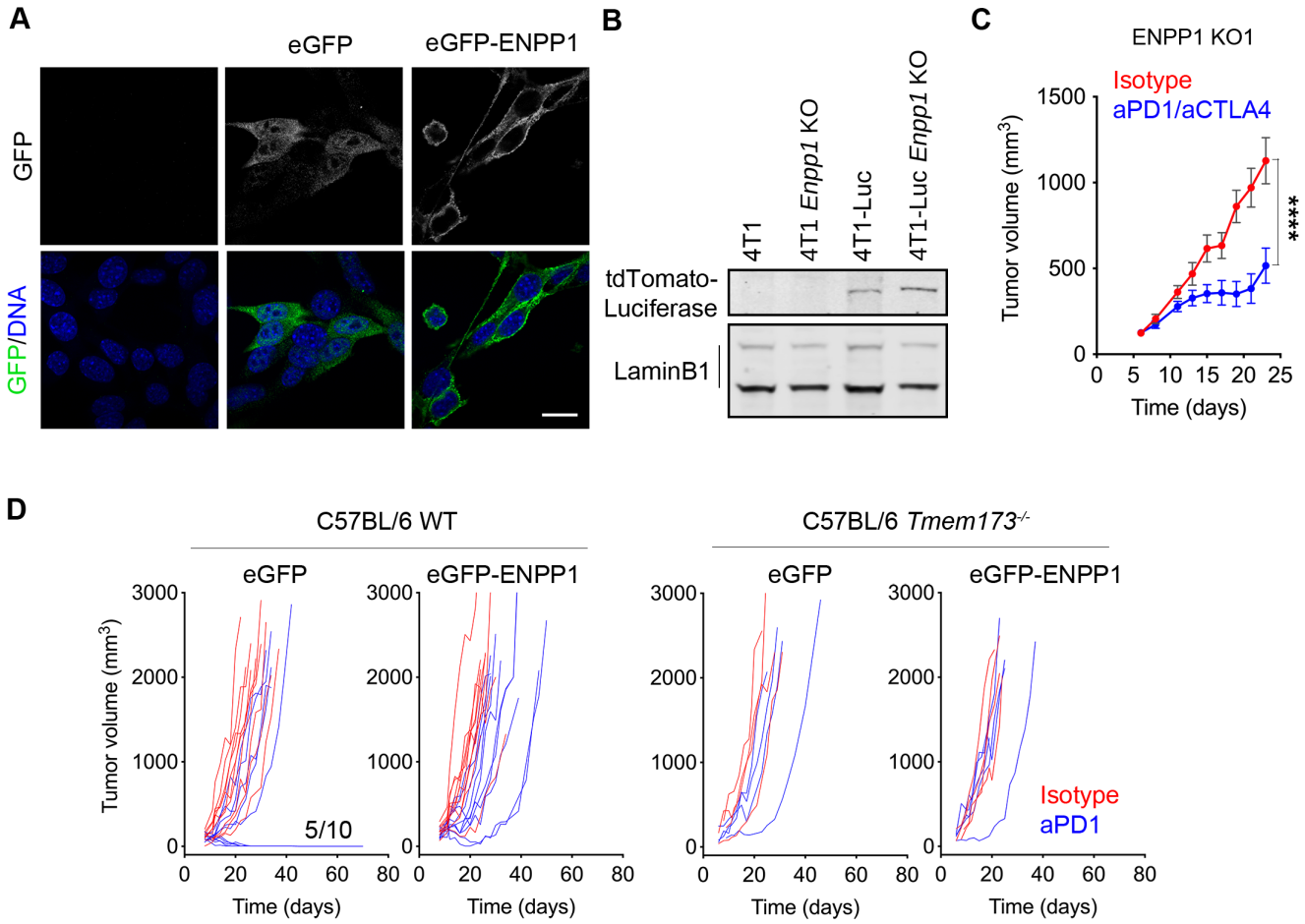

Supplementary Figure S6. (A) Representative immunofluorescence images of control, eGFP-expressing, and eGFP-ENPP1 expressing CT26 cells stained using DAPI (DNA), scale bar 10μm. (B) Immunoblots of control and luciferase expressing wildtype or *Enpp1*-KO 4T1 cells stained using anti-tdTomato-Luciferase and Lamin B1 antibodies. (C) Growth of wildtype or *Enpp1*-KO 4T1 tumors derived from an independent KO cell clone different from the one shown in Figure 4, datapoints represent mean ± s.e.m., n = 15 animals per group, **** $p < 0.0001$, two-sided t-test. (D) Spider plots of eGFP or eGFP-ENPP1 expressing E0771 orthotopic tumors inoculated in WT or *Tmem173*$^{-/-}$ C57BL/6 hosts.

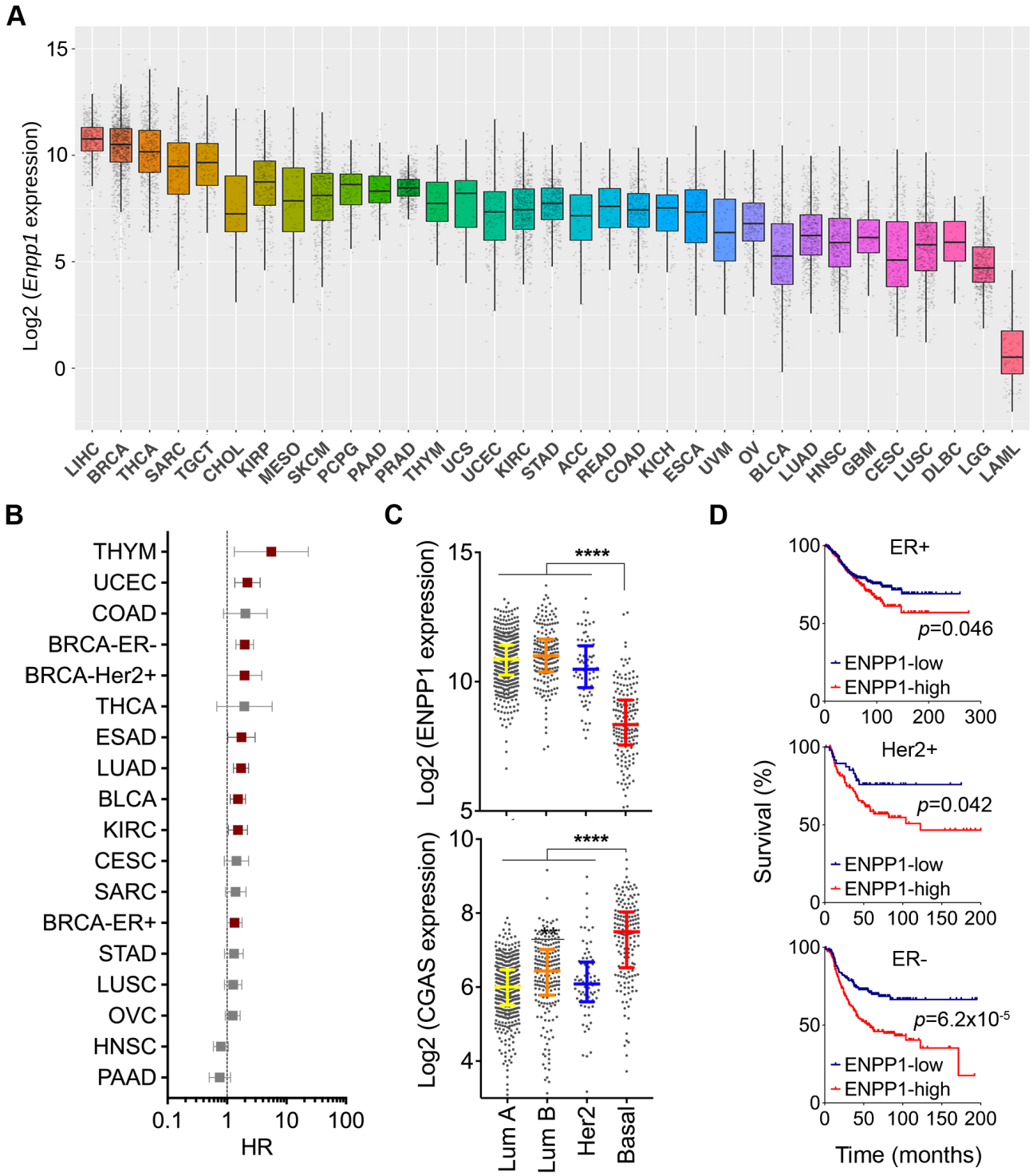

Supplementary Figure S7. (A) ENPP1 mRNA levels across human cancer types found in the TCGA database. (B) Hazard ratio for death of patients stratified by tumor ENPP1 median expression values. Data points represent HR ± 95% CI, red data points represent $p < 0.05$. (C) *CGAS* and *ENPP1* mRNA expression levels across breast cancer subtypes found in the TCGA, bars represent median ± interquartile range, ** $p<0.01$, **** $p<0.0001$, two-sided Mann-Whitney test. (D) Overall survival of breast cancer patients stratified by tumor receptor status and ENPP1 expression levels, significance tested using log-rank test.

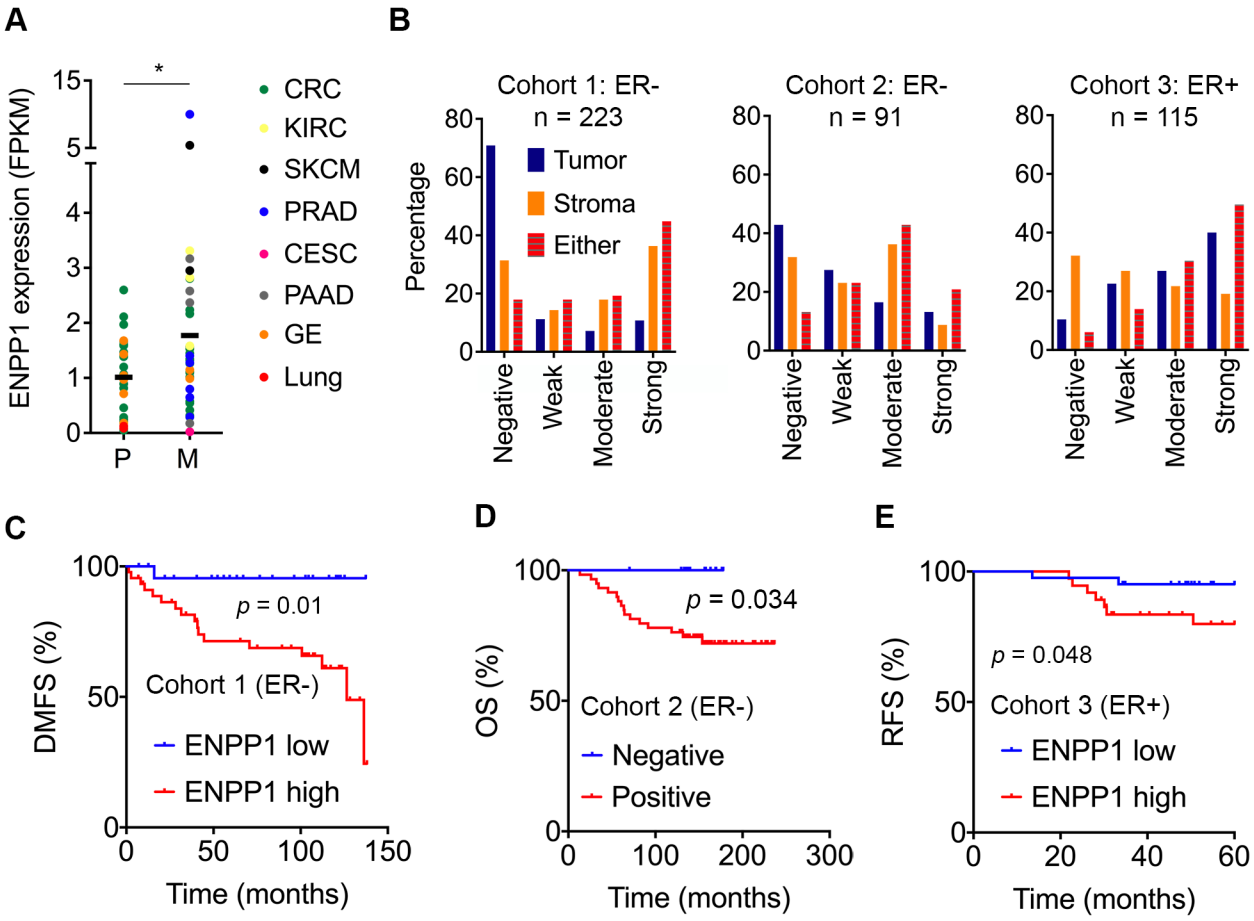

Supplementary Figure S8. (A) ENPP1 mRNA expression levels across human tumor-derived organoids. Bars represent median values, * $p < 0.05$, two-sided t-test. (B) Distribution tumor samples exhibiting stroma-specific and cancer cell-specific staining patterns of ENPP1 in three independent cohorts of human breast cancer. (C-E) Distant metastasis-free survival (DMFS, C), Overall survival (OS, D), and relapse-free survival (RFS, E) in patients with TNBC (C-D) or ER+ breast cancer (E) stratified based on their ENPP1 expression n = 69 (C), 73 (D), and 78 (E) patients, significance tested using log-rank test.

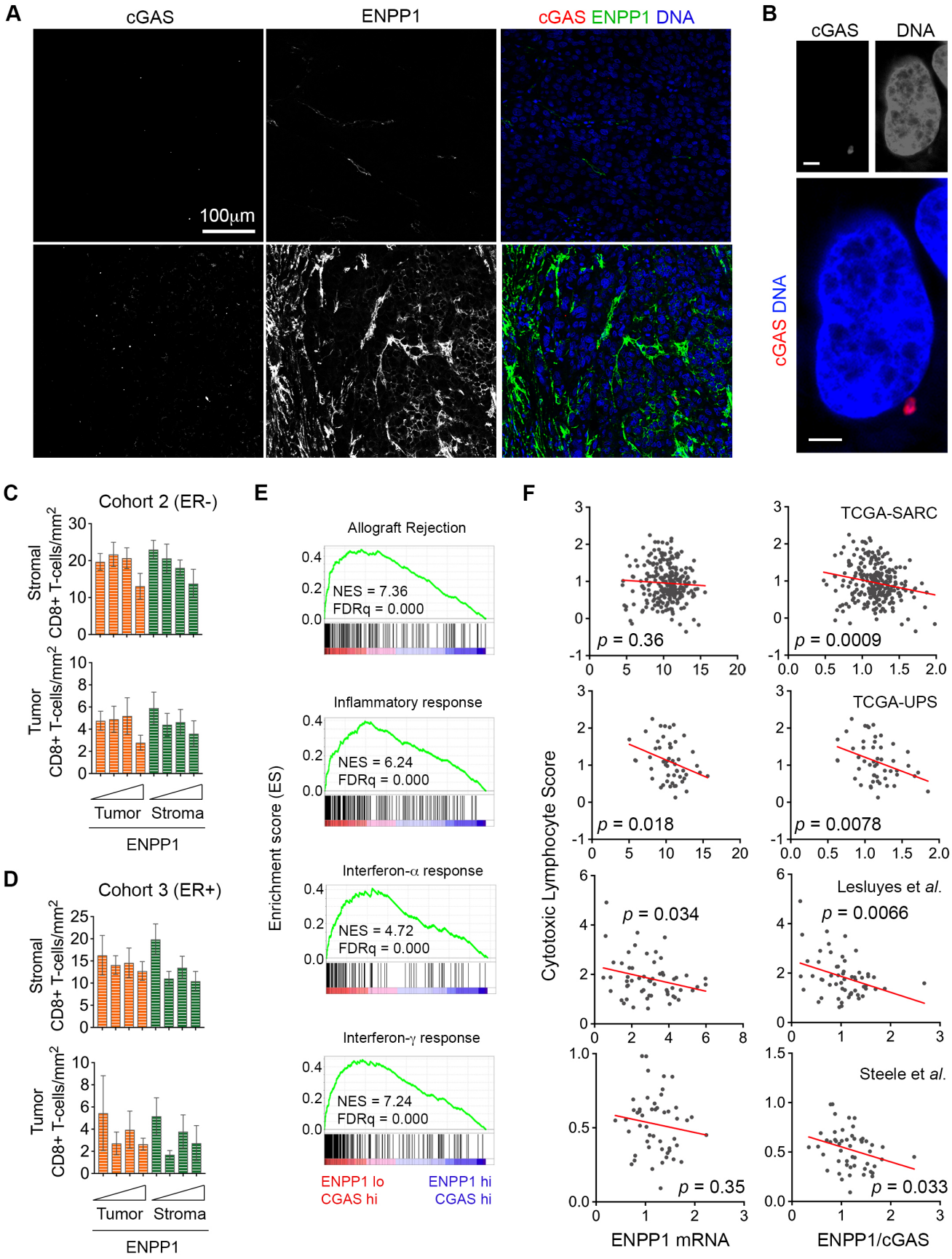

Supplementary Figure S9. (A) Representative immunofluorescence images of mucosal melanoma samples stained for using

DAPI (DNA), anti-cGAS antibody, and anti-ENPP1 antibody, sale bar 100□m. (B) A representative high-resolution immunofluorescence image of a mucosal melanoma sample stained using DAPI (DNA) or anti-cGAS antibody showing cGAS localization to micronuclei. Scale bar 2μm. (C-D) Percentage of tumor or stromal CD8+ T-cells two independent human breast cancer cohorts stratified based on their tumor and stromal ENPP1 expression. (E) Gene-set enrichment plots comparing cGAS^{high}-ENPP1-^{high} and cGAS-^{high}ENPP1-^{low} human breast tumors showing upregulation of inflammation related gene sets in ENPP1-low tumors. (F) Correlation between cytotoxic lymphocyte score and either ENPP1 levels or the ratio of ENPP1-to-cGAS mRNA levels in 3 independent sarcoma datasets.

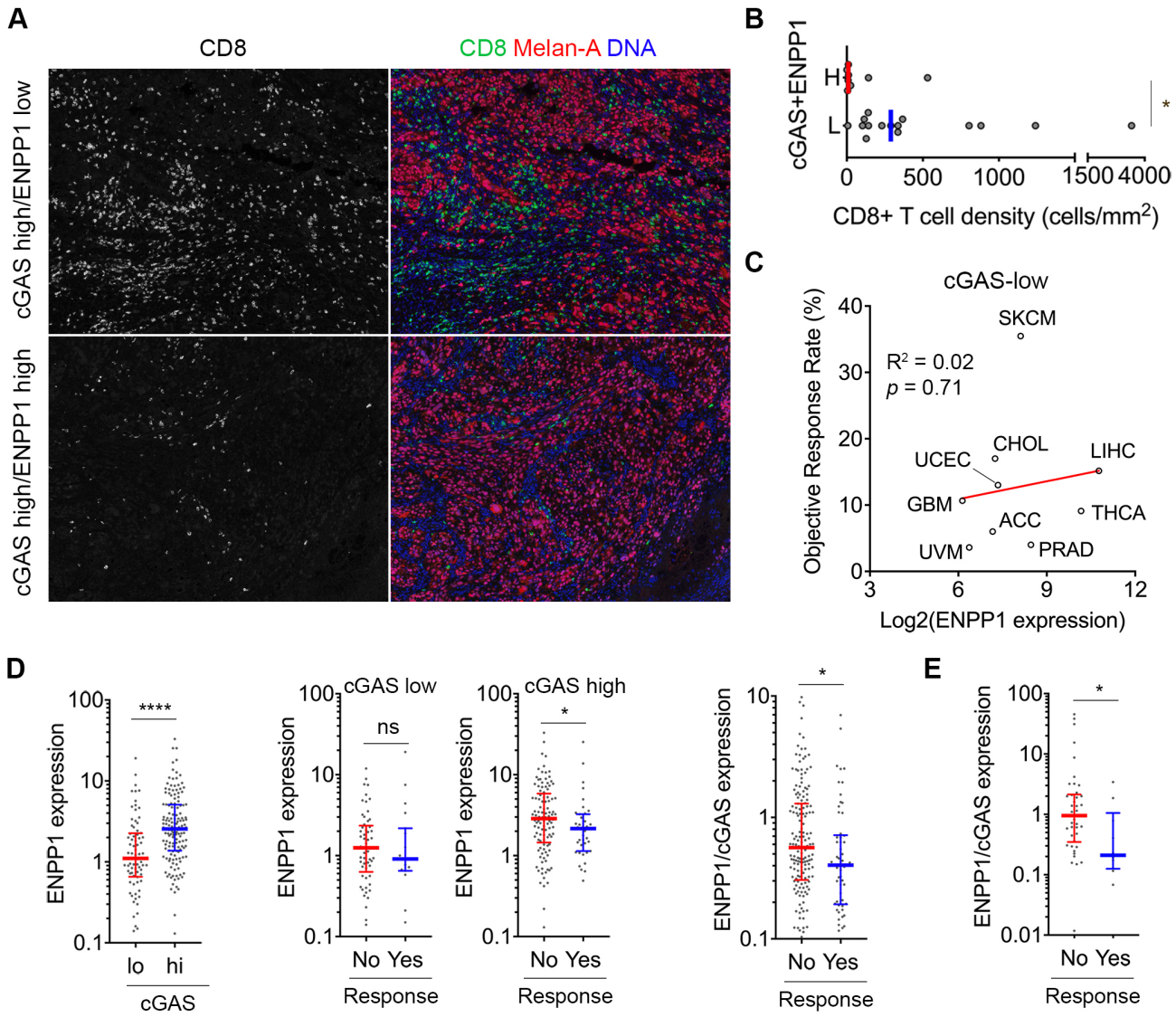

Supplementary Figure S10. (A) Representative multispectral immunofluorescence images of mucosal melanoma samples stained using DAPI (DNA), anti-CD8, and anti-Melan A antibodies. (B) CD8+ T-cell density as a function of combined cGAS and ENPP1 staining intensity in mucosal melanoma samples. Scale bar 100 μm. Bars represent median, *p<0.05 two-sided Mann-Whitney test. (C) Percent objective response rate (ORR) to anti-PD1/PD-L1 therapy by cancer type in tumor histologies with low levels of *Cgas* expression. (D-E) ENPP1 and cGAS mRNA expression levels of in bladder tumors (D) or TNBC (E) stratified by response to ICB. Bars represent median ± interquartile range, * p<0.05, **** p<0.0001, two-sided Mann-Whitney test.

Supplementary Table S1. crRNA guide sequences

Gene target	crRNA vs. shRNA	Catalog number
Enpp1	crRNA	GATTCCGGATAAAGTCCCTA
Cgas	crRNA	GCGAGGGTCCAGGAAGGAAC
Nt5e	crRNA	TGAATAAGATCATCGCCCTG
Sting	crRNA	CTACATAACAACATGCTCAG
Enpp1	shRNA	TTAATAATCTTCTCTTCTGCCA
Enpp1	shRNA	TTTCAATAAAAAATCATTCCAC
Enpp1	shRNA	TTAGAGACAATTATATTCCGTA
Enpp1	shRNA	TATTAAATAATTTTGAGTTGTA

Supplementary Table S2. Antibodies used in immunoblots

Antibodies against	Company	Catalog number
mouse cGAS	Cell Signaling Technology	31659
β-Actin	Abcam	ab6276
STING	Cell Signaling Technology	13647
α-Tubulin	Sigma-Aldrich	T9026
Lamin B1	Abcam	ab16048
human ENPP1	Abcam	ab223268
human ENPP1	Abcam	ab40003
Nt5e	Cell Signaling Technology	13160

Supplementary Table S3. Antibodies used in immunofluorescence

Antibodies against	Company	Catalog number
human ENPP1	Abcam	ab223268
human centromere proteins	Antibodies Incorporated	15-234-0001
mouse cGAS	Cell Signaling Technology	31659
GFP	Sigma-Aldrich	11814460001

Supplementary Table S4. Antibodies used in immunohistochemistry

Antibodies against	Company	Catalog number
human ENPP1	Abcam	ab40003
human ENPP1	Abcam	ab223268
CD45	BD Pharmingen	550539
CD8α	Cell Signaling Technology	98941
NK1.1	Thermo Fisher Scientific	MA1-70100
human cGAS	LifeSpan BioSciences	LS-C757990
Melan-A	Santa Cruz Biotechnology	sc-20032

Supplementary Table S5. Antibodies used in flow cytometry

Antibodies against	Company	Catalog number
CD45, APC-eFluor 780	Thermo Fisher Scientific	47-0451-82
Ly6G, APC	Thermo Fisher Scientific	17-9668-82
CD4, PE-Texas Red	Thermo Fisher Scientific	MCD0417
F4/80, PE/Cy5	BioLegend	123112
CD8, PE	Tonbo Biosciences	50-0081-U500
CD11b, PE/Cy7	Thermo Fisher Scientific	25-0112-82
CD3ε, BV785	BioLegend	100355
PD1, APC/Cy7	BioLegend	135224

SUPPLEMENTARY REFERENCES

1. Tozbikian G, Brogi E, Kadota K, Catalano J, Akram M, Patil S*, et al.* Mesothelin expression in triple negative breast carcinomas correlates significantly with basal-like phenotype, distant metastases and decreased survival. PLoS One **2014**;9(12):e114900 doi 10.1371/journal.pone.0114900.
2. Salgado R, Denkert C, Demaria S, Sirtaine N, Klauschen F, Pruneri G*, et al.* The evaluation of tumor-infiltrating lymphocytes (TILs) in breast cancer: recommendations by an International TILs Working Group 2014. Ann Oncol **2015**;26(2):259-71 doi 10.1093/annonc/mdu450.

3. Parkes EE, Walker SM, Taggart LE, McCabe N, Knight LA, Wilkinson R*, et al.* Activation of STING-Dependent Innate Immune Signaling By S-Phase-Specific DNA Damage in Breast Cancer. J Natl Cancer Inst **2017**;109(1) doi 10.1093/jnci/djw199.
4. Mulligan JM, Hill LA, Deharo S, Irwin G, Boyle D, Keating KE*, et al.* Identification and validation of an anthracycline/cyclophosphamide-based chemotherapy response assay in breast cancer. J Natl Cancer Inst **2014**;106(1):djt335 doi 10.1093/jnci/djt335.
5. Gyorffy B, Lanczky A, Eklund AC, Denkert C, Budczies J, Li Q*, et al.* An online survival analysis tool to rapidly assess the effect of 22,277 genes on breast cancer prognosis using microarray data of 1,809 patients. Breast Cancer Res Treat **2010**;123(3):725-31 doi 10.1007/s10549-009-0674-9.
6. Gyorffy B, Surowiak P, Budczies J, Lanczky A. Online survival analysis software to assess the prognostic value of biomarkers using transcriptomic data in non-small-cell lung cancer. PLoS One **2013**;8(12):e82241 doi 10.1371/journal.pone.0082241.
7. Yarilin D, Xu K, Turkekul M, Fan N, Romin Y, Fijisawa S*, et al.* Machine-based method for multiplex in situ molecular characterization of tissues by immunofluorescence detection. Sci Rep **2015**;5:9534 doi 10.1038/srep09534.
8. Cancer Genome Atlas Research Network. Electronic address edsc, Cancer Genome Atlas Research N. Comprehensive and Integrated Genomic Characterization of Adult Soft Tissue Sarcomas. Cell **2017**;171(4):950-65 e28 doi 10.1016/j.cell.2017.10.014.
9. Steele CD, Tarabichi M, Oukrif D, Webster AP, Ye H, Fittall M*, et al.* Undifferentiated Sarcomas Develop through Distinct Evolutionary Pathways. Cancer Cell **2019**;35(3):441-56 e8 doi 10.1016/j.ccell.2019.02.002.
10. Bray NL, Pimentel H, Melsted P, Pachter L. Near-optimal probabilistic RNA-seq quantification. Nat Biotechnol **2016**;34(5):525-7 doi 10.1038/nbt.3519.
11. Soneson C, Love MI, Robinson MD. Differential analyses for RNA-seq: transcript-level estimates improve gene-level inferences. F1000Res **2015**;4:1521 doi 10.12688/f1000research.7563.2.
12. Becht E, Giraldo NA, Lacroix L, Buttard B, Elarouci N, Petitprez F*, et al.* Estimating the population abundance of tissue-infiltrating immune and stromal cell populations using gene expression. Genome Biol **2016**;17(1):218 doi 10.1186/s13059-016-1070-5.
13. Rooney MS, Shukla SA, Wu CJ, Getz G, Hacohen N. Molecular and genetic properties of tumors associated with local immune cytolytic activity. Cell **2015**;160(1-2):48-61 doi 10.1016/j.cell.2014.12.033.
14. Dobin A, Davis CA, Schlesinger F, Drenkow J, Zaleski C, Jha S*, et al.* STAR: ultrafast universal RNA-seq aligner. Bioinformatics **2013**;29(1):15-21 doi 10.1093/bioinformatics/bts635.
15. Li B, Dewey CN. RSEM: accurate transcript quantification from RNA-Seq data with or without a reference genome. BMC Bioinformatics **2011**;12:323 doi 10.1186/1471-2105-12-323.